3. THE THERMODYNAMICS OF SEA ICE

You are in a Swedish icebreaker entering Independence Fjord, the great ice-choked fjord of Northeast Greenland that was named by Robert Peary and was the site of the 1906 tragedy in which the explorer Mylius Erichsen perished with all his men. It is a foggy day in summer. The ship comes to a halt in the heavy ice. As the morning mist clears you take a helicopter further up the fjord in search of a type of ice that you have read about but never seen, ***sikussak.*** *In 1945 Lauge Koch, the revered Danish explorer and surveyor of East Greenland, completed a monumental work on "The East Greenland Ice", a book upon which he had lavished five years of his life whilst interned by the Germans. He had found a few places in the furthest northern reaches of the island where the fast ice remains for decades and becomes immensely thick. The Eskimos, who have a word for every type of ice and snow, call it sikussak,"fjord ice that looks like ocean ice". At last you see it, a wild landscape like the Grand Canyon, formed by the annual cycle of melt and refreezing, with mesas, isolated peaks and spires, and deep gullies filled with running water. A dozen or so melt streams like this radiate out from a thaw hole, like the legs of a spider, but beware of the hole itself — a turbulent mass of fresh water plunges down it into the sea below. If you fell you would never be found. The helicopter drops you and your colleagues and the coring equipment. You begin to drill from a mesa, carefully slicing each core into 10 cm sections which you put into bottles to melt later and measure the salinity. You are 6 m down and nowhere near the bottom. Suddenly the helicopter returns. The ship must leave and sail east to meet the King of Sweden who is flying out by long-range helicopter from Svalbard. You cannot argue with royalty. Reluctantly you pack up and leave. You will never know the thickness reached by sikussak.*

How thick does sea ice grow if left alone for years? Will it grow thicker from year to year or does it reach a limit? If this limit exists, how does it vary in different parts of the world? How is it affected by snow fall and heat flux from the ocean? These are questions which can be addressed by relatively simple models, and which we consider in this chapter.

3.1. THERMOPHYSICAL PROPERTIES OF SEA ICE

Before we start we must examine the basic thermal properties of sea ice, which determine

its rates of growth and decay, and especially the phase transitions that occur during melting and freezing. The properties which we need to know are the thermal conductivity, specific heat, latent heat of fusion, and extinction coefficient for radiation. We need to know these properties both for sea ice and for snow, since the snow which covers the sea ice in winter plays an important role in limiting the thickness to which sea ice can grow; its low thermal conductivity makes it act like a thermal blanket which reduces heat loss from the surface of the ice.

Sea ice is a mixture of four components: ice; liquid brine; air bubbles; and solid salts. The conduction of heat through sea ice is influenced both by the porosity (air bubble content) of the ice and by the solid salt content, but the most complex effect occurs with liquid brine. This is because, as we have seen in chapter 2, the brine is contained in tiny cells of concentrated solution; each cell is at its freezing point and is in phase equilibrium with the surrounding ice. When the temperature within the ice rises the ice surrounding the brine cell melts, absorbing latent heat, diluting the brine and raising its freezing point to the new temperature. When the ice temperature falls some of the water in the cell freezes, releasing latent heat and producing a smaller cell containing more concentrated brine with a lower freezing point. The brine cell is thus a **thermal reservoir,** retarding the heating or cooling of the ice. This extra resistance to warming or cooling means that the specific heat of sea ice is a function both of salinity (increasing with increasing salinity) and temperature (increasing with temperature, since the brine volume becomes very large near the melting point).

3.1.1. Thermal Conductivity

The thermal conductivity of sea ice was first investigated by Malmgren (1927) as part of his classic work done during Amundsen's "Maud" expedition. Later work has included theoretical studies by Schwerdtfeger (1963) and Shuleikin (1968) and experimental work by Nazintsev (1964) and Ono (1965), with a review of results by Doronin and Kheisin (1977).

Untersteiner (1961) introduced an approximate formula for thermal conductivity, which was later employed in the model of Maykut and Untersteiner (1971) described in section 3.3. His relationship was

$$k_i = k_o + \beta S_i / T_i \qquad (3.1)$$

where k_i is thermal conductivity; k_o is the thermal conductivity of pure polycrystalline ice at temperature T_i (°C); S_i psu is the salinity of the ice; and $\beta = 0.13$ W m^{-1}. The thermal conductivity of pure ice was given by Yen (1981) as

$$k_o = 9.828 \exp(-0.0057\ T) \qquad (3.2)$$

where T, the ice temperature, is now in °K. k_o has units W m^{-1} °K^{-1}. Yen's formula for pure ice was based on extensive experimentation by many researchers. Equation (3.1), on the other hand, is rather a crude approximation since it has been found that k_i is strongly dependent not only on the salinity of the ice (as expressed in 3.1) but also on its air bubble content. It is a reasonable approximation for use in models which deal only with salinity.

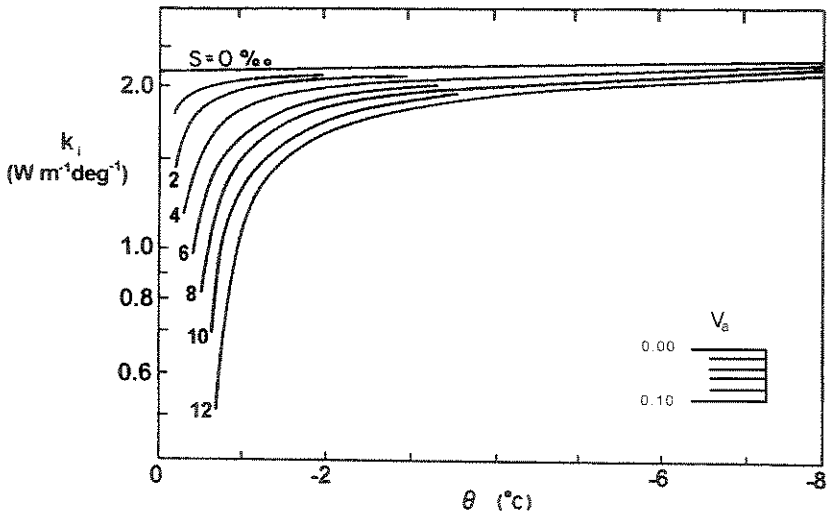

Figure 3.1. Thermal conductivity of sea ice as a function of salinity and air bubble content (after Ono, 1968).

The question of air bubble content was considered in the studies of both Schwerdtfeger (1963) and Ono (1968). The problem is that the thermal conductivity of seawater brine (the constituent of the brine cells) is about 25% that of pure ice, while the thermal conductivity of air is less than 1% that of ice. The result is that the thermal conductivity of typical sea ice is greatly reduced relative to that of pure ice near the melting point, when the brine volume is high, but as the temperature is lowered reaches an asymptote similar to the thermal conductivity of pure ice *so long as there are no air bubbles.* The air bubble content lowers this asymptote. The first theoretical model, that of Anderson (1958), considered only brine cells, which he allowed to occur either as isolated random spheres or as cylinders or layers oriented as discussed in chapter 2 at right angles to the c-axis. Schwerdtfeger (1963) added randomly distributed spherical air bubbles in the ice to this model. Finally Ono (1968) allowed the air bubbles to be distributed through both the ice and the brine.

We present Ono's (1968) model results (fig. 3.1) as being the most easy to use. The main curves are for bubble-free ice, and it is very clear how salinity depresses the thermal conductivity near the melting point but not at lower temperatures. To account for the effect of air bubbles one takes the bubble-free value and reduces the thermal conductivity by the bubble fraction V_a shown on the inset curve.

Fig. 3.1 shows that very saline, warm ice (e.g. young ice forming in early winter, or melting first-year ice) has a very much lower thermal conductivity than cold or low-salinity ice, by a factor of up to 2 or 3. This is seldom taken into account in discussions of growth or melt rates, but both of these will be significantly retarded in warm salty ice if the model is correct. Of course, none of the models to date take account of possible convection in the liquid or gaseous phases, and we might expect convection in brine drainage channels, for instance, to significantly increase the average thermal conductivity of warm saline ice.

Finally, no measurements have been done on the relationship between k_i and crystal orientation, although the model of Anderson (1958) predicts that the conductivity parallel to the c-axis is much lower than the conductivity perpendicular to the c-axis. If confirmed experimentally, this would provide another reason, in addition to the energetic argument given in chapter 2, why crystals with c-axes horizontal grow faster than their competitors — the latent heat of fusion can be conducted away more easily.

3.1.2. Specific Heat

The specific heat c_i of sea ice was found by Ono (1967) to give a good fit to the following empirical relationship:

$$c_i = c_o + a\ T_i + b\ S_i / T_i^2 \tag{3.3}$$

where $c_o = 2113$ J kg^{-1} °C^{-1} is the specific heat of pure ice, T_i is temperature in °C, S_i psu is ice salinity, $a = 7.53$ J kg^{-1} °C^{-2} and $b = 0.018$ MJ °C kg^{-1}. The third term on the right hand side shows that the effects of temperature and salinity on specific heat are mainly important near the melting point, and are insignificant below –8°C.

A quantity which is easier to measure directly is **thermal diffusivity**, σ_i, defined as

$$\sigma_i = k_i / (\rho_i\ c_i) \tag{3.4}$$

This was calculated by Ono (1968) with results shown in fig. 3.2. It is a directly observable thermal property in that it can be calculated from the rate of change of the temperature profile in an ice sheet. Methods of calculating σ_i are discussed in Ono (1965, 1968) and Yen (1981), and observations made by Ono (1965, 1968), Lewis (1967) and Weller (1968) have agreed quite well with predictions.

3.1.3. Latent Heat of Fusion

The concept of latent heat in the case of sea ice is a complex one, since thermodynamically it is possible for sea ice and brine to coexist at any temperature, and therefore for sea ice to melt at temperatures other than 0°C if it is bathed in a suitably concentrated salt solution, such as occurs at the walls of brine cells when brine cell migration is taking place (section 2.4).

Ono (1968) produced a formula based on thermodynamic considerations and suitable for use at temperatures above –8°C, where complicating factors set in on account of the precipitation of solid sodium sulphate ($Na_2SO_4.10H_2O$) from concentrated brine. His formula is

$$q = 333394 - 2113\ T_i - 114.2\ S_i + 18040\ (S_i/T_i) \tag{3.5}$$

where q is the latent heat of fusion in J kg^{-1}, T_i is temperature in °C, and S_i psu is ice

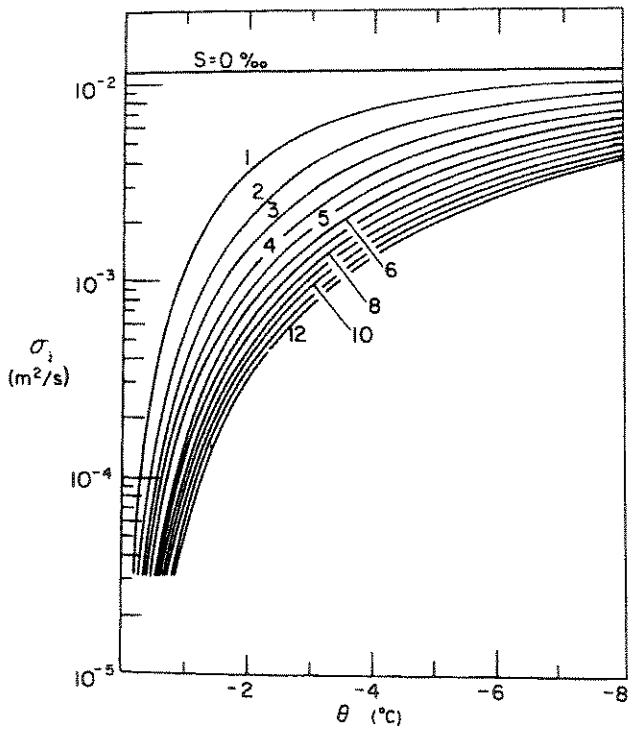

Figure 3.2. Thermal diffusivity of sea ice as a function of salinity and temperature (after Ono, 1968).

salinity. Ono carried out laboratory experiments to test both (3.5) and (3.3), but with results which showed that at times of freeze, melt or rapid temperature change, the brine in sea ice is seldom in equilibrium with the ice itself. These formulae should therefore be applied with caution, and as in so many other aspects of basic sea ice physics, more experimentation needs to be done.

Further discussion of latent heat is given by Doronin and Kheisin (1977), and table 3.1 shows some values of q for temperatures close to 0°C.

Table 3.1. Heat q in kJ required for complete fusion of 1 kg of sea ice.

T_i °C	S_i psu					
	0	1	2	4	6	8
–0.5	335	300	264	194	124	53
–1.0	336	318	301	266	230	195
–2.0	338	329	320	302	284	264
–3.0	340	334	328	316	303	291

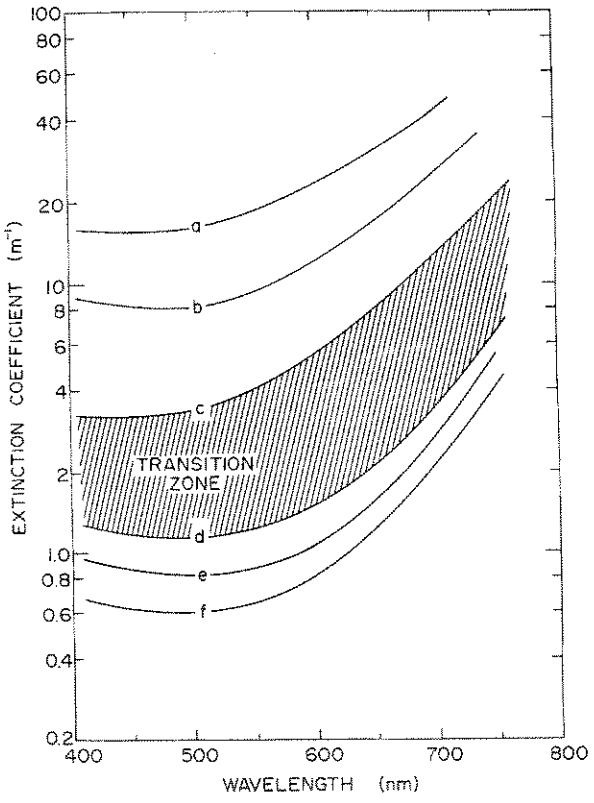

Figure 3.3. Spectral extinction coefficients for various types of ice and snow: (a) dry compact snow, (b) melting snow, (c) the surface layer of melting multi-year ice, (d) the interior of multi-year ice (the area marked "transition zone" representing transitional layers between surface and deep interior), (e) the interior of first-year ice, (f) ice beneath an old melt pond (after Grenfell and Maykut, 1977).

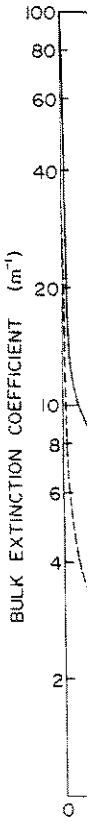

Figure 3.4. Bulk extinct
free) ice (dashed curve). A

3.1.4. Radiation Extinction Coefficient

When solar radiation is incident on an ice or snow cover, a fraction of it is immediately reflected. This is called the **albedo** (α). The rest penetrates into the interior, where it is subject to absorption and scattering. The rate of absorption depends on the angle of incidence of the radiation and the wavelength as well as the properties of the material. For any wavelength, however, the decay of penetrating energy with distance is found to be exponential (**Beer's Law**), and if we think in terms of penetration through a vertical distance z in the snow or ice cover, can be represented in terms of a **spectral extinction coefficient** $\kappa(z,\lambda)$, i.e.

$$I(z,\lambda) = I_0(\lambda) \exp\left(-\int_0^z \kappa \, dz\right) \tag{3.6}$$

where $I(z,\lambda)$ is the intensity of radiation penetrating to a depth z in the material and $I_0(\lambda)$ is the net radiation penetrating into the surface, given by

Here F_0 is the net to
The spectral extinc
some experimental re
than in ice, and there
the red, hence the ten
think in terms of e-fo
of its initial value), w
(blue) to 8 metres at
For the purposes
an unnecessary comp
with wavelength, and
by weighting the sp
shortwave spectrum

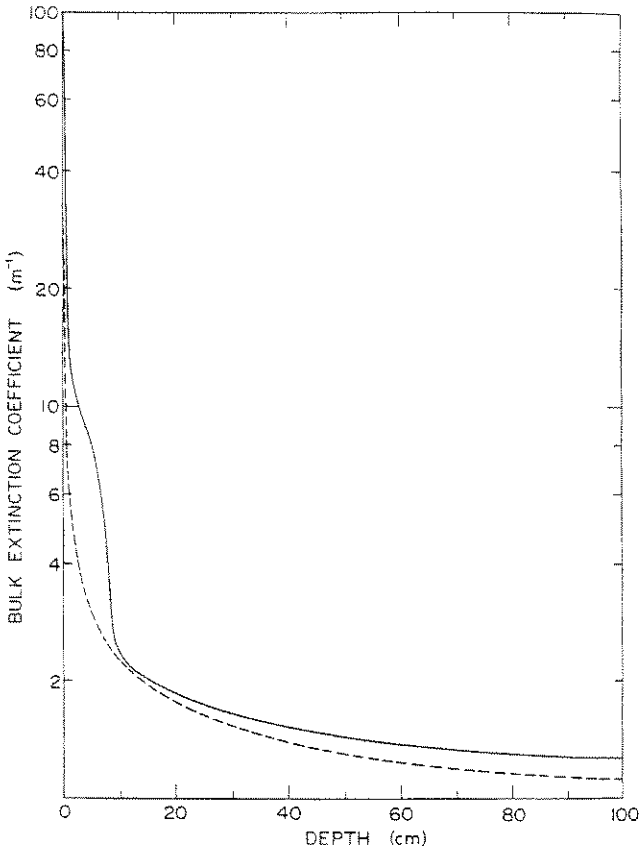

Figure 3.4. Bulk extinction coefficients in multi-year ice (solid curve) and first-year blue (i.e. mainly bubble-free) ice (dashed curve). After Grenfell and Maykut, 1977.

$$I_0(\lambda) = \int_0^\infty (1 - \alpha)\, F_0(0,\lambda)\, d\lambda \qquad (3.7)$$

Here F_0 is the net total shortwave radiation at the surface.

The spectral extinction coefficient varies enormously between ice types. Fig. 3.3 shows some experimental results. Clearly radiation is extinguished much more rapidly in snow than in ice, and there is a lower extinction rate at the blue end of the spectrum than at the red, hence the tendency for ice to look blue when viewed by transmitted light. If we think in terms of e-folding distances (the distance to reduce the intensity to 1/e, i.e. 37%, of its initial value), we find these varying for typical sea ice from 24 metres at 470 nm (blue) to 8 metres at 600 nm (red) to 2 m at 700 nm (near infra-red) (Perovich, 1998).

For the purposes of thermodynamic modelling, as we shall show in section 3.3, it is an unnecessary complication to have to deal with the variation of extinction coefficients with wavelength, and instead we simply use a **bulk extinction coefficient** κ_z, obtained by weighting the spectral extinction coefficient by the distribution of energy in the shortwave spectrum which reaches penetration z, i.e.

$$\kappa_z = \frac{\int \kappa(z,\lambda)\ I(z,\lambda)\ d\lambda}{\int I(z,\lambda)d\lambda} \tag{3.8}$$

where the integration is carried out over the spectral range which carries all the significant shortwave radiation.

Fig. 3.4 shows bulk extinction coefficients derived in this way for two kinds of ice. Note how the values are highest in the uppermost 20 cm of the ice cover, and then decline to typical values of 1 to 1.5 m^{-1} for interior ice. Much higher values have been found for snow: 4.3 m^{-1} for dense Antarctic snow (Weller and Schwerdtfeger, 1967) up to 40 m^{-1} for freshly fallen snow (Thomas, 1963).

The use of bulk extinction coefficients has been criticised in recent years (e.g. Maykut *et al.*, 1992; Perovich, 1998) because they do not depend entirely on the properties of the ice. They depend on the spectral properties of the albedo, the sky conditions on the day of measurement (sunny days have a relatively greater longwave component in the incident spectrum than cloudy days), and are strongly dependent on conditions in the upper few cm of the ice cover, which therefore take on a critical importance for heat budget estimates.

Albedo, too, should properly be expressed as a **spectral albedo** $\alpha(\lambda)$, and this quantity has been measured for many kinds of ice (Maykut, 1986; Maykut *et al.*, 1992; Perovich, 1998). However, once again for heat budget models it is more convenient to define a bulk albedo in an analogous way to (3.8), i.e.

$$\alpha = \frac{\int \alpha(\lambda)\ I(0,\lambda)\ d\lambda}{\int I(0,\lambda)d\lambda} \tag{3.9}$$

Area-averaged bulk albedo is a highly variable quantity and is particularly difficult to define in summer, when the surface is a mixture of snow-covered ice, bare ice, melting ice and melt pools. At this time of year albedo is most difficult to predict, yet in models it is most important to get the value correct in summer, since incident radiation is greatest then (Curry *et al.*, 1995). Fig. 3.5 shows the wide range of values obtained for different ice types, ranging from 0.87 for new snow down to 0.15 for an old melt pond (and 0.06 for open water, which is also prevalent in summer and which does affect the ice mass budget through lateral melting of floes in water which has undergone surface warming). This variability is one of the greatest problems in ice thermodynamics. The most recent field study to address this problem was SHEBA (Surface Heat Budget of the Arctic), a 1997–8 drift experiment in which a single area of ice was followed through changing seasons (Moritz and Perovich, 1996). It is clear that the additional precision of using spectral albedos in models is not justified while the bulk albedo is so poorly known.

3.2. EARLY MODELS OF ICE GROWTH AND DECAY

Many early attempts were made to develop empirical relationships to predict ice growth from observed air temperatures. The best known were by Barnes (1928), Lebedev (1938) and Zubov (1945). Zubov, in his classic work, *L'dy Arktiki (Arctic Ice)*, found the relationship

Figure 3.5. Range of
(1954), Chernigovskiy (

(3.8)

all the significant

two kinds of ice.
r, and then decline
have been found
eger, 1967) up to

ears (e.g. Maykut
the properties of
conditions on the
component in the
litions in the upper
ce for heat budget

), and this quantity
l., 1992; Perovich,
nt to define a bulk

(3.9)

rticularly difficult
, bare ice, melting
dict, yet in models
adiation is greatest
ained for different
elt pond (and 0.06
ffect the ice mass
surface warming).
s. The most recent
t of the Arctic), a
through changing
precision of using
so poorly known.

predict ice growth
3), Lebedev (1938)
ic Ice), found the

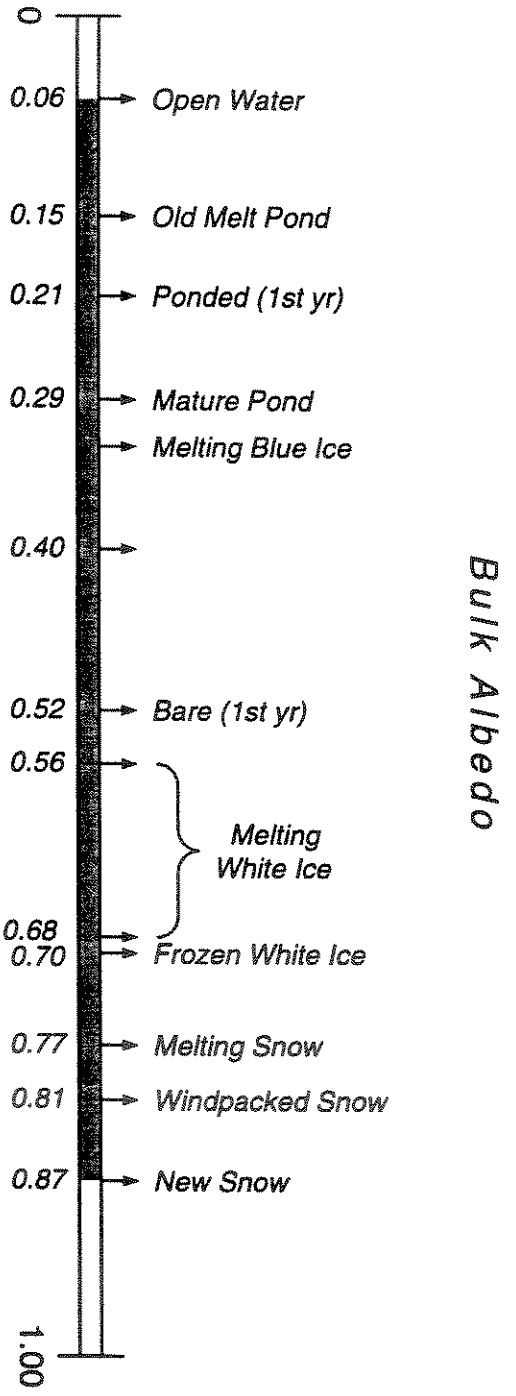

Figure 3.5. Range of observed values for bulk albedo of sea ice (after Perovich, 1998). Data are from Burt (1954), Chernigovskiy (1963), Langleben (1971), Grenfell and Maykut (1977) and Grenfell and Perovich (1984).

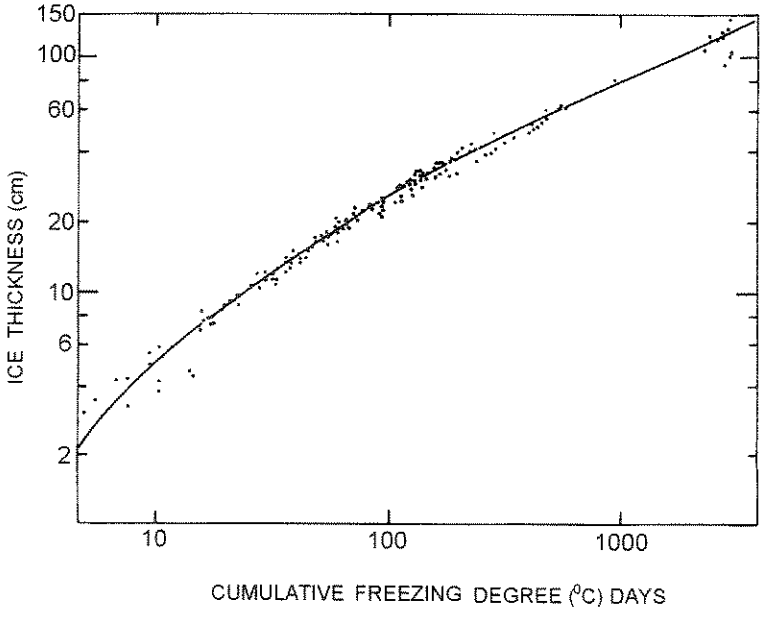

Figure 3.6. Anderson's (1961) relationship for young ice thickness as a function of degree-days of cold.

$$H^2 + 50\ H = 8\ \theta \tag{3.10}$$

where H is ice thickness in cm, and θ is cumulative freezing degree-days. Lebedev's relationship was

$$H = 1.33\ \theta^{0.58} \tag{3.11}$$

Both these authors used the concept of cumulative degree-days of cold during the winter. The average daily temperature is subtracted from –1.8°C (the freezing point of sea water) and summed from day to day. The result was found to give a good correlation with the thickness reached by sea ice, with a complicating effect from the snow cover (which inhibits ice growth).

More recent work on such semi-empirical relationships includes Bilello (1961), who developed a statistical method based on observations of fast ice growth, and Anderson (1961), who derived a relationship for young ice in the Arctic with minimum snow cover (fig. 3.6), which fitted the relation

$$H^2 + 5.1\ H = 6.7\ \theta \tag{3.12}$$

Bilello (1961, 1980) developed a similar technique to predict ice decay in summer for nearshore data, obtaining

$$\Delta H = 0.55\ \theta' \tag{3.13}$$

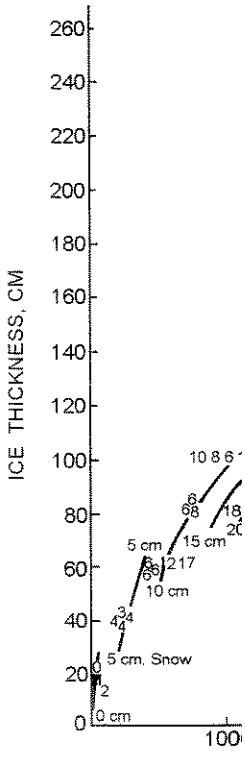

Figure 3.7. Family of c
Bilello, 1961).

where ΔH is the tota
days above the freez

These techniques
the water is so shallo
work well for young
the conductive flux i
to interpret the best a
and Sinha, 1981). T
climate change upon
are inadequate for de
cover. Anderson's (1
than about 80 cm bec
a family of curves (f
do not expect equatic
warm winds from la

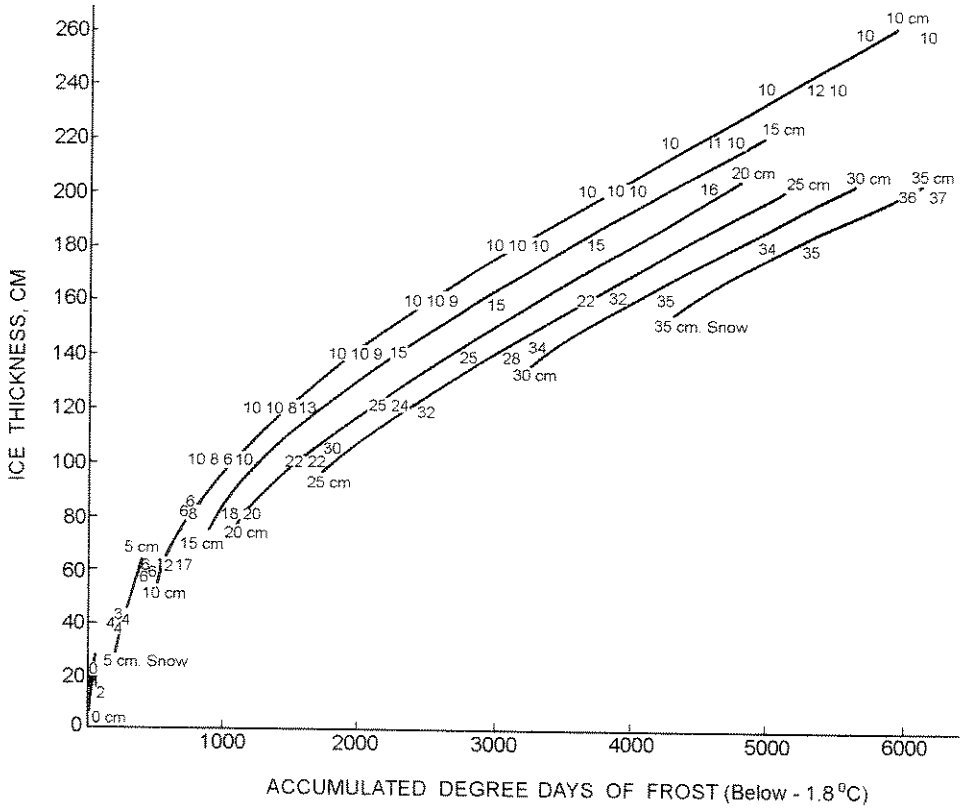

Figure 3.7. Family of curves of ice thickness versus degree-days of cold, for different snow depths (after Bilello, 1961).

degree-days of cold.

(3.10)

e-days. Lebedev's

(3.11)

l during the winter.
point of sea water)
orrelation with the
now cover (which

Bilello (1961), who
wth, and Anderson
nimum snow cover

(3.12)

ecay in summer for

(3.13)

where ΔH is the total decrease in ice thickness in cm and θ' is the cumulative degree-days above the freezing point.

These techniques work for fast ice because there is no ocean heat flux involved, since the water is so shallow that it consists of only one layer of polar surface water; they also work well for young ice in refreezing leads because during the early stages of growth the conductive flux in the ice greatly exceeds the oceanic heat flux. They have been used to interpret the best and longest series of fast ice growth data from a whole winter (Nakawo and Sinha, 1981). They are good semi-quantitative indicators of the likely impact of climate change upon the fast ice zone, as we shall discuss in chapter 8. However, they are inadequate for describing thicker ice in the deep ocean, or ice which carries a snow cover. Anderson's (1961) data deviated greatly from his equation at higher thicknesses than about 80 cm because of the variable snow cover, while Bilello (1961) had to develop a family of curves (fig. 3.7) to allow for differences due to snow cover. In addition, we do not expect equation 3.13 for decay rate to be valid anywhere except near shore, where warm winds from land may act, since out in the main polar pack ice zone the summer

air temperature always stays very near 0°C. Maykut (1986) showed how relationships of the type (3.10) to (3.12) based on degree-days of cold may be developed on simple theoretical grounds, provided one makes highly simplifying assumptions such as

— a uniform slab of ice with constant thermal conductivity;
— no ocean heat flux;
— crudely parameterised heat exchange at ice surface, proportional to temperature difference between ice surface and air;
— imposed snow layer of constant thickness.

It was clear that a more complete modelling approach based on a full physical theory was required. It is worth mentioning here the very first attempt at such a theory, since it occurred very early, in fact not very long after the radiation law itself was discovered. In 1890 Stefan developed a simple model which showed that the thickness H of young ice should follow the relations

$$H \propto t^{1/2} \tag{3.14}$$

and

$$dH/dt \propto (T_a - T_w) / H \tag{3.15}$$

where t is time and T_a and T_w are the temperatures of the top and bottom of the ice. The growth rate should decrease rapidly as the ice becomes thicker, by about an order of magnitude between ice 10 cm and 100 cm thick in the case of the Arctic Ocean.

This model brings out the main properties of ice thermodynamics: that ice growth slows as the ice gets thicker, so that an icefield in which leads have opened because of divergent wind stress tries to "heal" itself through rapid ice growth in the refreezing leads, and that under thermodynamics alone an icefield composed of ice of varying thicknesses tries to reach a uniform thickness value, with thin ice getting thicker and thick ice getting thinner. However, it still does not take proper account of radiative forcing at the top of the ice, nor of the variability of ice conductivity, nor energy exchanges with the ocean. Clearly a more complete model is necessary.

3.3. THE MAYKUT-UNTERSTEINER MODEL

In 1971 a model was produced for the thermodynamic growth and decay of sea ice in the Arctic Ocean by Maykut and Untersteiner. It is still the basis for understanding the thermodynamics of sea ice, with a simplified version suitable for climate studies being presented by Semtner (1976) and modifications based on more recent data by Maykut (1986). A more recent reassessment and update has been by Ebert and Curry (1993).

3.3.1. Formulation

The model considers the seasonal cycle of short and long-wave radiation fluxes upon a growing or decaying ice sheet, with a seasonally specified snowfall and a given oceanic heat flux. We assume that the ice sheet is an infinite, horizontally homogeneous slab, with

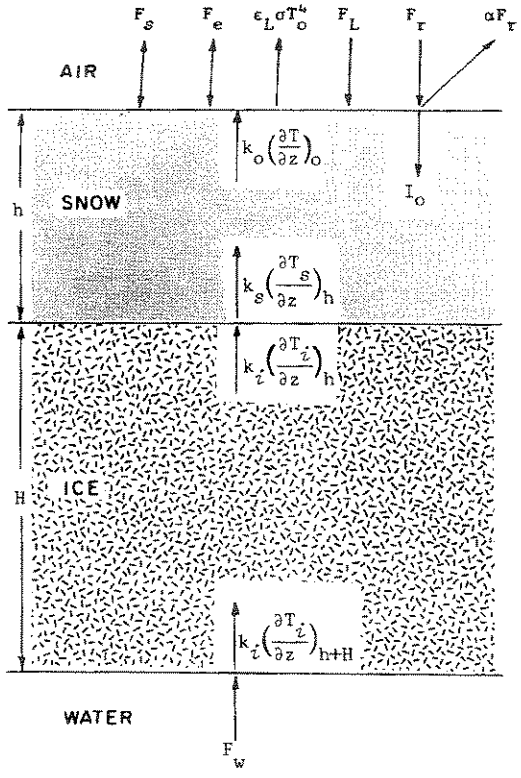

Figure 3.8. Fluxes in a uniform snow-covered ice sheet (after Maykut and Untersteiner, 1971).

no thickness variations due to ice deformation, and that the ocean upon which it floats is at rest so that there is no heat transfer due to friction between the water and the ice. The ice transfers heat between the ocean and the atmosphere by conduction, but this transfer is affected by brine cells within the ice and by short-wave radiation penetrating the upper surface of the ice during spring, summer and autumn. The snow cover also reduces both the radiative and conductive transfer of heat through the slab and so must be represented as a second layer within the model.

Figure 3.8 shows the geometry and the fluxes involved. A snow layer of thickness h covers a sea ice sheet of thickness H. We assume that mass changes and energy absorption happen only at the snow and ice boundaries. At the top boundary of the snow (or of bare ice in summer), the snow or ice may melt, but mass can be added only through snowfall. At the ice-water interface either ablation (ice melt) or accretion (ice growth) may take place. We consider the heat balance at each boundary in turn, and also the heat transmission in the interior of the snow and the ice. The sign convention is that energy fluxes are considered positive towards a surface and negative away from a surface. The vertical axis z is measured downwards from the snow surface.

Upper surface of snow

We start at the top of the snow layer. Here we have a balance of energy fluxes, where several incoming energy fluxes from the atmosphere are balanced by long-wave radiation from the surface and by heat penetrating into the ice. The incoming radiations are:-

F_r = incoming short-wave radiation from the sun which reaches the surface after penetrating the atmosphere.

F_L = incoming long-wave radiation from the atmosphere and clouds, which themselves have absorbed some incoming solar radiation as it passed through the atmosphere, and have re-emitted it at a lower frequency by virtue of their own absolute temperature.

The outgoing radiations are:-

αF_r = the fraction of incoming solar radiation which is immediately reflected by the snow surface. α is the albedo of the surface.

$e_L \sigma T_o^4$ = the outgoing long-wave radiation emitted by the surface. Here T_o is the absolute temperature of the snow surface, σ is the **Stefan-Boltzmann constant** ($= 5.671 \times 10^8$ W m^{-2} K^{-4}) and ε_L is the **long-wave emissivity.** This is simply an expression of the Stefan-Boltzmann law of radiation, which states that the total radiation emitted by a body is proportional to the fourth power of its absolute temperature. σ is the constant of proportionality involved, while the emissivity expresses the way in which the colour or texture of a surface causes it to emit less than the theoretical maximum amount of radiation, called "black body radiation". For snow, the emissivity is usually close to unity, and for sea ice it lies in the range 0.66 to 0.99 (Cavalieri *et al.*, 1981).

There are two additional energy flux terms which can be positive or negative. These are:-

F_s = sensible heat flux to the adjacent air. Sensible heat is the heat actually physically transferred by the snow surface to the overlying air by conduction. If the snow surface is warmer than the air near the surface, the heat transfer is upwards and the sensible heat is negative; if it is colder the heat transfer is downwards and the sensible heat is positive. Sensible heat transfer is a complex process since upward sensible heat involves creating small-scale turbulent convection as the heated parcels of air move upwards and are replaced by colder air parcels moving downwards to interact in their turn with the surface.

F_l = latent heat flux to the adjacent air. This is the energy exchange due to sublimation of snow into water vapour.

If we examine the fluxes downwards from the snow surface into the body of the snow layer, there are two:-

I_o = the flux of radiative energy which penetrates through the snow surface into the body of the snow. This was considered in section 3.1.4.

F_c = the heat conducted downwards into the snow layer (or upwards from the snow layer to the snow surface). This is given by

$$F_c = k_s \, (\partial T / \partial z)_o \tag{3.16}$$

where k_s is the thermal conductivity of the snow and $(\partial T/\partial z)_o$ is the temperature gradient through the snow measured at the snow surface z = 0.

If the surface temperature T_o is below the freezing point, these fluxes will all balance, with the balance determining the value of T_o. If, however, the surface of the snow is at the melting point, an imbalance between the incoming and outgoing energy fluxes can be accommodated through the melting of snow, causing a change in h (or of H is the ice surface is bare). Thus there are two possible equations for the energy balance, depending on the surface temperature:-

$$(1 - \alpha) \, F_r - I_o + F_L - \varepsilon_L \, \sigma \, T_o^4 + F_s + F_l + k_s \, (\partial T / \partial z)_o = 0 \quad \text{if} \quad T_o < 273.16$$

or

$$= - \, [q \, d(h + H) / dt]_o \quad \text{if} \quad T_o = 273.16 \tag{3.17}$$

where q is the latent heat of fusion of the surface material, whether it be snow or bare ice.

Most of the parameters used in equation (3.17) are external, seasonally varying parameters which have to specified based on our knowledge of environmental conditions in the Arctic or Antarctic Ocean (α, F_r, F_L, F_s and F_l). Other parameters require a knowledge of snow or ice properties (k_s, q, ε_L), while snow deposition, which is a partial determinant of h, must also be specified as an external input to the system.

Interior of snow layer

Inside the snow layer, assuming that there is one (in summer this component of the model is of zero thickness and so is ignored), heat is conducted along the temperature gradient from warm to cold, while at the same time the penetrating solar radiation is gradually absorbed. The absorption of radiation by snow is a complex process dependent on wavelength, angle of incidence, and the physical structure of the snow. It was considered in section 3.4, and is here expressed for simplicity in terms of a single bulk extinction coefficient κ_s, such that the flux I(z) at a depth z is given by

$$I(z) = I_o \exp (- \kappa_s \, z) \tag{3.18}$$

The thermal conductivity of the snow, k_s, is also assumed to be constant.

Consider a small unit cell within the snow, of dimensions δx, δy, δz (figure 3.9). The flux incident on the upper surface of the cell is

$$F_1 = - \, k_s \, (\partial T/\partial z)_z + I_o \exp \, [- \kappa_s \, z] \tag{3.19}$$

The flux emerging from the lower surface is

$$F_2 = - \, k_s \, (\partial T/\partial z)_{z+\partial z} + I_o \exp \, [- \kappa_s \, (z + \partial z)] \tag{3.20}$$

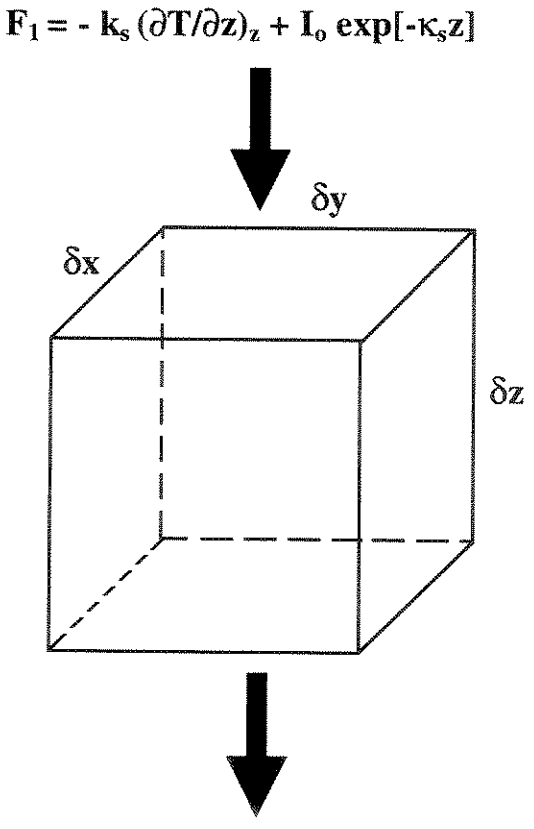

Figure 3.9. Schematic of heat conduction through a unit cell of the snow or ice cover.

The net rate of energy gain by the cell is $(F_1 - F_2)\ \delta x\ \delta y$, which can be equated to the rate of temperature rise in the cell by

$$(F_1 - F_2)\ \delta x\ \delta y = \rho_s\, c_s\ \delta x\ \delta y\ \delta z\ (\partial T/\partial t)_z \qquad (3.21)$$

where c_s is the specific heat of the snow and ρ_s is its density. Assuming a slow rate of change of temperature gradient with distance, and neglecting terms above second order, this yields

$$\rho_s\, c_s\ (\partial T/\partial t)_z = \kappa_s\, I_o\, \exp\,[-\kappa_s\, z] + k_s\ (\partial^2 T/\partial z^2)_z \qquad (3.22)$$

Snow-ice interface

Assuming that a snow layer exists, we can also assume that conduction is continuous

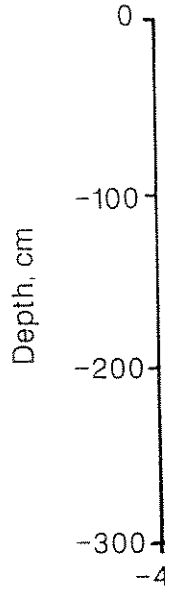

Figure 3.10. Temperature
floe of multi-year sea ice

through the boundary

where k_i is the therm
$(\partial T_i/\partial z)_h$ are the tempe
Because snow is a mu
profile through snow
the gradient being mu
to map the thicknesse
of closely-spaced ther
point at which the ter
the upper and lower s
zero. This does not w
is at or near 0°C. Figu
multi-year ice in the

Interior of sea ice la

Inside the sea ice lay

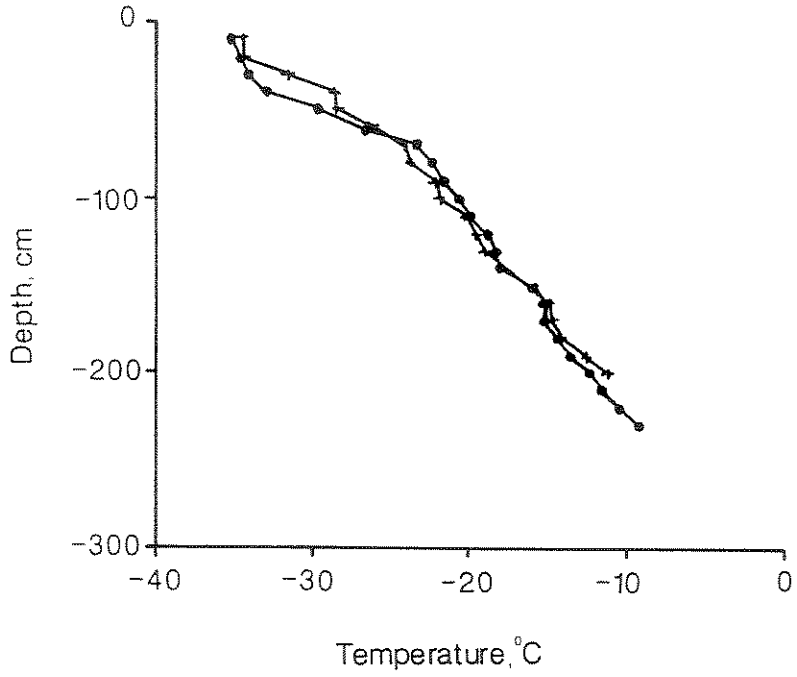

Figure 3.10. Temperature profiles obtained by author using two thermistor chains inserted through the same floe of multi-year sea ice NW of Svalbard, March 19 1993.

through the boundary between the snow and the ice, so that

$$k_s (\partial T_s/\partial z)_h = k_i (\partial T_i/\partial z)_h \tag{3.23}$$

where k_i is the thermal conductivity of the top part of the ice layer and $(\partial T_s/\partial z)_h$ and $(\partial T_i/\partial z)_h$ are the temperature gradients just above and just below the interface respectively. Because snow is a much poorer conductor of heat than ice this means that a temperature profile through snow-covered ice in winter changes its slope at the snow-ice interface, the gradient being much greater above than below the interface. This provides a means to map the thicknesses of snow and ice through a winter automatically. A vertical chain of closely-spaced thermistors is installed through the ice sheet, feeding a data logger. The point at which the temperature profile changes its gradient is the snow-ice interface, while the upper and lower surfaces of the system are the points at which the gradient becomes zero. This does not work in summer when the whole atmosphere-snow-ice-water system is at or near 0°C. Figure 3.10 shows a temperature gradient obtained by the author through multi-year ice in the Arctic Ocean during March; the gradient changes at about 60 cm.

Interior of sea ice layer

Inside the sea ice layer the same conduction and absorption processes occur as inside the

snow layer, so the governing equation is the same as (3.22) but substituting ice for snow, i.e.

$$\rho_i c_i (\partial T/\partial t)_z = \kappa_i I_o \exp [-\kappa_i z] + k_i (\partial^2 T/\partial z^2)_z \quad (3.24)$$

where κ_i is now the extinction coefficient within the ice.

However, as we have shown in section 3.1, both the specific heat and the thermal conductivity of sea ice are functions of both temperature and salinity. Therefore a single value cannot be used for either $(\rho_i c_i)$ or k_i, but both must be expressed in terms of ice salinity $S_i(z)$, itself a function of depth within the ice, and temperature T_i. We have discussed appropriate formulations for these quantities in section 3.1; Maykut and Untersteiner chose to adopt simple approximate formulae due to Untersteiner (1961):

$$k_i = k_o + \beta S_i / T_i \quad (3.25)$$

and

$$\rho_i c_i = (\rho c)_p + \gamma S_i / T_i^2 \quad (3.26)$$

where S_i psu is ice salinity, T_i °C is ice temperature, $\beta = 0.13$ W m^{-1}, k_o is given by (3.2), $(\rho c)_p$ is the pure ice value of 1.944 MJ m^{-3} °K^{-1}, and $\gamma = 17.15$ MJ kg^{-1} °K. These relationships should be substituted into eqn. (3.24).

Ice-water interface

At the interface between the ice and the ocean there are only two fluxes, the turbulent heat flux from the ocean into the ice F_w, and the conductive heat flux in the ice close to the boundary. At the interface either freezing or melting may occur, depending on whether the ocean heat flux dominates (melting) or the conductive heat flux dominates (freezing). During winter one expects the conductive heat flux to dominate because the temperature gradient through the ice between the water and the atmosphere is so high, so that ice growth will occur. Nevertheless, if the ice is thick enough the temperature gradient will be reduced to the point where melting may occur instead. Here we see the physical justification for the concept of **equilibrium thickness** of an ice sheet: if some process (such as ridging) generates ice of greater than the equilibrium thickness, the ice will begin to melt at the bottom even in the middle of winter, and even while thinner ice in the vicinity is growing. Recent results show, however, that the Maykut-Untersteiner theory gives too low a melt rate for very thick ice in ridges, which probably ablates through hydrodynamic effects or mechanical erosion.

The equation expressing the heat balance at the ice bottom is:-

$$k_i (\partial T_i/\partial z)_{h+H} - F_w = [q\, d(h + H) / dt]_{h+H} \quad (3.27)$$

In principle F_w can be expressed in terms of the gradient of water temperature T_w just below the ice-water interface, the density ρ_w and specific heat c_w of the near-surface water, and a so-called **coefficient of eddy diffusivity** K_w in the water column under the ice, a function of its degree of turbulence:-

$$F_w = \rho_w c_w [K_w (\partial T_w \partial z)]_{h+H} \quad (3.28)$$

However, in practice
be derived from large
yields the upward flo
Steele and Boyd, 199
lost to the atmosphere
temperature variation.
It is therefore not ne

3.3.2. Input Param

Maykut and Unterste
were a function of ti
was rerun until a st
achieved. The fluxes
stations up to that da
some exception such
marise them as follo

F_r was derived fro
is zero from N
month^{-1} in June
F_L, derived from th
highest in July
F_s, derived from D
a maximum in
in spring and s
F_j, also from Doro
strongly negati
I_o is set at 50 MJ
means that 17%
κ_i, the extinction
1961; Chernigo
F_w was set at 2 W
Panov (1964) a
for the Eurasia
α is set at high v
ice without mel
just at a time w
assumes its gre
and melt ponds
bare ice and me
used an averag
high.

Snow deposition, a p
of 30 cm betv
November 1 to

However, in practice these quantities are hard to determine while the heat flux itself can be derived from larger scale oceanographic profiling of temperature and salinity, which yields the upward flow of heat from the thermocline into the near-surface layers (e.g. Steele and Boyd, 1998). To a first approximation, this heat flow can be assumed to be lost to the atmosphere (although some heat is stored in the upper layers to give a seasonal temperature variation, most important in the Antarctic) and so can be identified with F_w. It is therefore not necessary to use equation (3.28).

3.3.2. Input Parameters

Maykut and Untersteiner ran their model with energy fluxes for the Arctic Ocean that were a function of time of year but repeated themselves in an annual cycle. The cycle was rerun until a steady annual pattern of temperature and thickness variation was achieved. The fluxes and parameters used were based on data obtained from drifting stations up to that date, and are still regarded as reasonable values for the Arctic, with some exception such as summer albedo, considered later in this chapter. We may summarise them as follows:-

F_r was derived from values proposed by Marshunova (1961) and Fletcher (1965). It is zero from November to February and rises to a maximum of 803 MJ m^{-2} $month^{-1}$ in June.

F_L, derived from the same sources, is lowest in February and March (431 MJ m^{-2}) and highest in July (799 MJ m^{-2}).

F_s, derived from Doronin (1963), is from snow surface to atmosphere in winter, with a maximum in January of 49 MJ m^{-2}, and from atmosphere to snow (or bare ice) in spring and summer, with a maximum of –19 MJ m^{-2} in May.

F_l, also from Doronin, is very slightly negative through the winter, then becomes more strongly negative in summer, reaching –29 MJ m^{-2} in June.

I_o is set at 50 MJ m^{-2} applied evenly through the snow-free period of the year, which means that 17% of net short-wave radiation is assumed to penetrate the ice.

κ_i, the extinction coefficient, was set at 1.5 m^{-1}, independent of depth (Untersteiner, 1961; Chernigovskii, 1966).

F_w was set at 2 W m^{-2}. This is based on calculations by Crary (1960), Badgley (1961), Panov (1964) and Untersteiner (1964). It has received confirmation (1–3 W m^{-2}), for the Eurasian Basin in the winter months, from Steele and Boyd (1998).

α is set at high values for autumn to spring (0.81–0.85) when fresh snow lies on the ice without melting. The problem occurs in summer, when the albedo is very variable just at a time when the incoming short-wave radiation is highest so that the albedo assumes its greatest importance. The albedo is reduced by the presence of bare ice and melt ponds, but a typical rough Arctic sea ice surface may possess snow patches, bare ice and melt ponds simultaneously in varied proportions. Maykut and Untersteiner used an average value for July of 0.64, but later authors have considered this too high.

Snow deposition, a partial determinant of h, is assumed to comprise a linear accumulation of 30 cm between August 20 and October 30, a linear increase of 5 cm from November 1 to April 30, and an additional 5 cm during May. This was based on

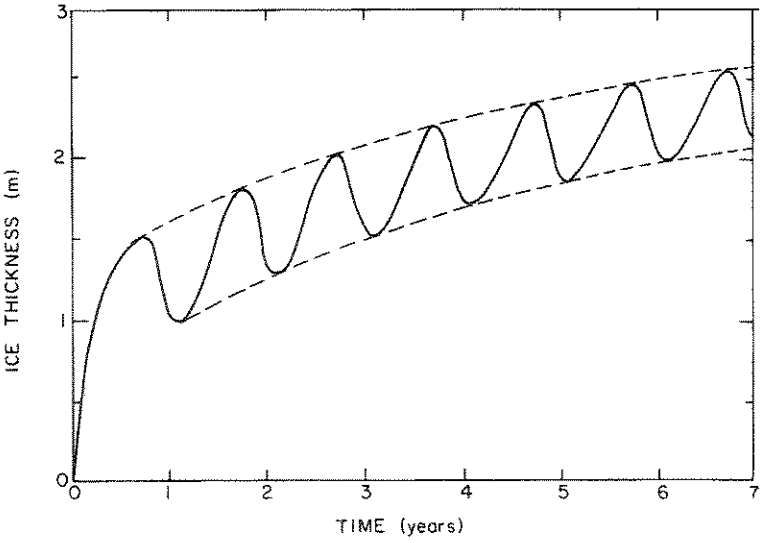

Figure 3.11. Pattern of thermodynamic ice growth in the central Arctic, assuming that an ice sheet begins to grow at the end of summer (time = 0) (after Maykut, 1986).

year-round measurements from US drifting stations (Untersteiner, 1961; Hanson, 1965). Snow density was set to 330 kg m^{-3} during the freezing season, and 450 kg m^{-3} once snow melt had begun.

S_i, ice salinity, affects thermal conductivity, specific and latent heats, and density. Maykut and Untersteiner used a standard profile, a function only of thickness, derived from Schwarzacher (1959).

3.3.3. Results

With heat budget values gathered in this way, the model predicts that a new ice sheet growing from open water at the beginning of winter reaches a thickness of 1.5 m in the first winter, then loses 0.5 m of thickness in summer from bottom and surface melt, with top surface melt making the greater contribution (fig. 3.11). If the ice is left to continue its evolution, subsequent annual growth and decay cycles enable it to approach an **equilibrium thickness** of 2.88 m, an asymptotic value about which the thickness oscillates on a seasonal basis (3.14 m in winter, 2.71 m in summer).

The subsequent annual cycling of the ice once it has reached its equilibrium thickness can in principle go on for ever, with a given parcel of ice gradually moving upwards through the ice sheet from year to year, since there is a net annual growth on the underside to cancel the net annual ablation of the top side. After many years the same ice floe exists but contains none of the ice with which it first started to grow; the skin of ice on the ocean is like human skin in this respect. The rate at which this upward movement happens

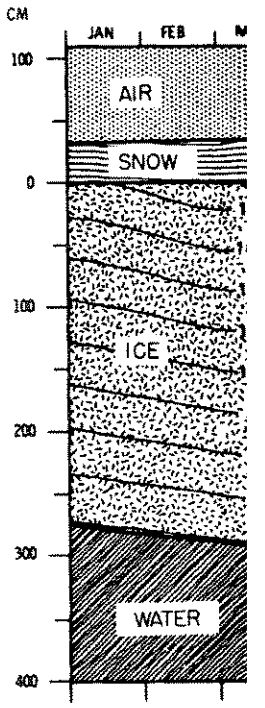

Figure 3.12. Predicted va
Untersteiner model. Isothe
2°C intervals. Melt at upp
accompanying hydrostatic

is important when we
such as oil introduce

In figure 3.12 we
8, and by June 29 all
19, by which time 4
which together creat
through the ice sheet
late August. During s
of ice at the bottom
equilibrium.

This is of course
year to year will caus
subArctic seas and f
ice is highly unlikely
thickness. However,
of sea ice thickness t
is sensitive to the va

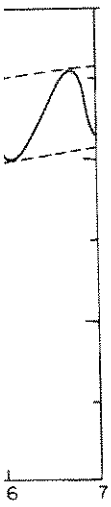

hat an ice sheet begins

ıer, 1961; Hanson,
season, and 450 kg

heats, and density.
only of thickness,

hat a new ice sheet
ıess of 1.5 m in the
d surface melt, with
:e is left to continue
: it to approach an
: thickness oscillates

quilibrium thickness
lly moving upwards
wth on the underside
: same ice floe exists
e skin of ice on the
l movement happens

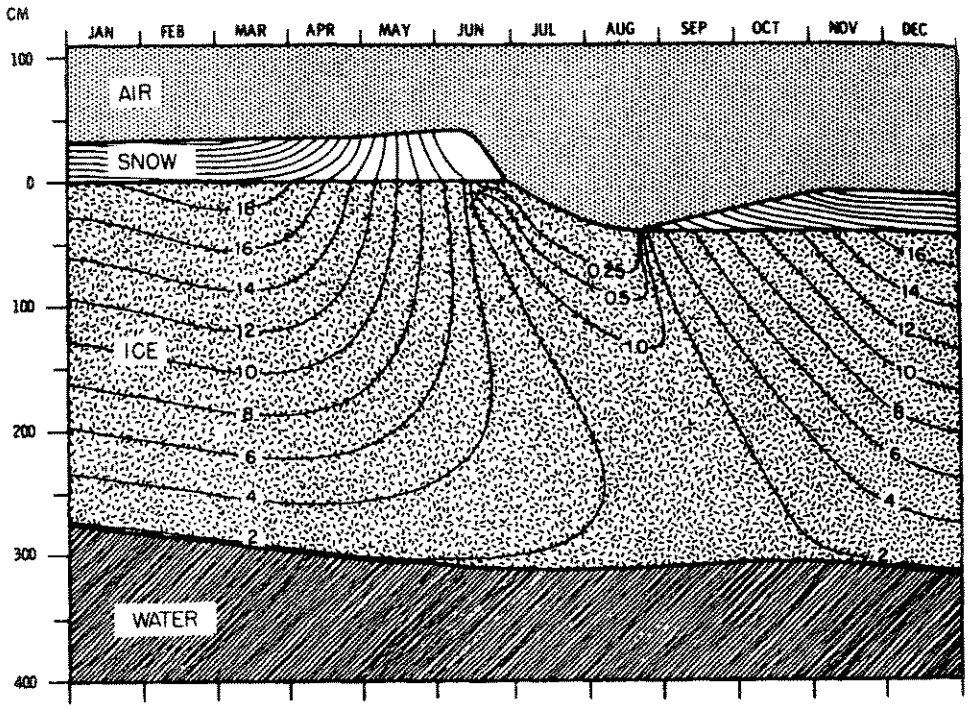

Figure 3.12. Predicted values of equilibrium temperature and thickness in central Arctic, according to Maykut-Untersteiner model. Isotherms in ice are labelled in negative °C; unlabelled isotherms in snow are drawn at 2°C intervals. Melt at upper ice boundary, and melt and growth at ice-water boundary, are shown without accompanying hydrostatic adjustment (after Maykut and Untersteiner, 1971).

is important when we consider how long it takes a sea ice sheet to rid itself of pollutants such as oil introduced at the bottom (see section 8.2.1).

In figure 3.12 we can see that there are some critical dates. Snow melt begins on June 8, and by June 29 all the snow has melted. Ice melt then begins and continues until August 19, by which time 40 cm of ice have melted off the top. This is the ice and the snow which together create the pattern of meltwater pools, and which can percolate down through the ice sheet flushing out remaining brine. New snow begins to accumulate in late August. During summer there is a small amount of bottom melt, but the winter growth of ice at the bottom must exceed this by about 40 cm in order to preserve an annual equilibrium.

This is of course an oversimplified picture. Variations in weather and snowfall from year to year will cause growth rates and equilibrium thicknesses to vary. The patterns for subArctic seas and for the Antarctic are also quite different, although in both cases sea ice is highly unlikely to survive (except as fast ice) for long enough to reach equilibrium thickness. However, the model results do demonstrate some very important sensitivities of sea ice thickness to changes in climatic forcing. In particular, the equilibrium thickness is sensitive to the values used for annual **snowfall** and for **oceanic heat flux**.

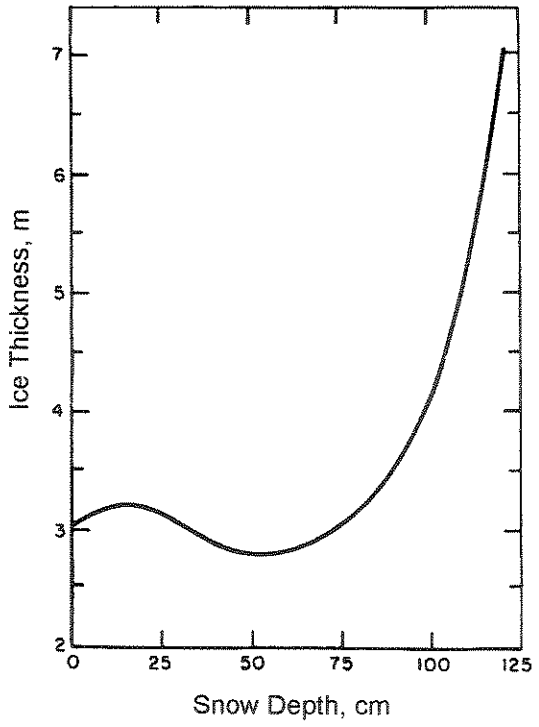

Figure 3.13. Average equilibrium thickness of Arctic sea ice as a function of maximum annual snow depth (after Maykut and Untersteiner, 1971).

Snow depth sensitivity

The sensitivity of equilibrium thickness to maximum annual snow depth is shown in fig. 3.13. The shape of the snowfall curve is due to the competing effects of snow as an insulator - which slows the rate of ice growth in winter - and snow as a covering material which melts off in early summer to reveal bare ice which can then develop a pattern of surface melt pools of low albedo, so enhancing the overall melt rate. The very high ice thicknesses caused by a thick snow cover occur when the snow becomes too thick to melt completely during the brief summer, so that surface melt pools cannot develop. At present the Arctic Ocean sits near the bottom of this curve, with a maximum annual snow depth of 30–50 cm, but if snowfall were multiplied by a factor of about 3 the ice would continue to grow indefinitely, with much of the extra thickness supplied by the snow itself which would grow thicker from year to year.

Ocean heat flux sensitivity

The sensitivity of equilibrium thickness to ocean heat flux is shown in fig. 3.14. The present value of F_w averaged over the Arctic Ocean is about 2 W m^{-2}; this is the value used, for instance, in the Hibler (1979) model of ice dynamics-thermodynamics (see

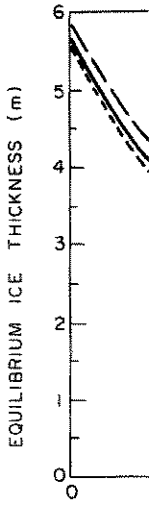

Figure 3.14. Average eq
flux. The dotted lines sho

chapter 4). Fig. 3.14
the ice would disap
the amount of heat t
if the Arctic thermocl
input from rivers at
can happen in the c

Other sensitivities

It has been suggeste
on ice, could be used
shows that if the sun
the equilibrium thick
ice to melt complet
probably not have s
much of the melt wa
wide darkening of th
winter, would be so
one of the more triv

A more obvious
and later heat balanc
summer air temperat
Arctic Ocean. Since
era of CO_2 doubling

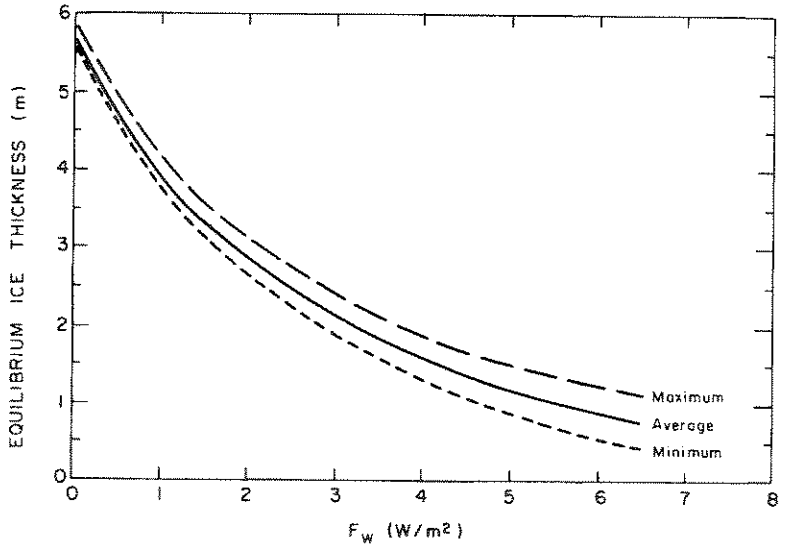

Figure 3.14. Average equilbrium thickness of Arctic sea ice as a function of the average annual oceanic heat flux. The dotted lines show annual maximum and minimum thicknesses (after Maykut, 1986).

chapter 4). Fig. 3.14 shows that if F_w increased to 7 W m^{-2}, with other factors unchanged, the ice would disappear completely. This might happen if there were a big increase in the amount of heat transported into the Arctic by the warm North Atlantic Current, or if the Arctic thermocline were to weaken or disappear because of a reduction in freshwater input from rivers at the surface. Similarly, if there were no oceanic heat flux at all, as can happen in the case of shallow water, the equilibrium thickness would rise to 6 m.

Other sensitivities

It has been suggested that an artificial reduction in albedo, e,g, by sprinkling coal dust on ice, could be used to reduce ice thickness and help clear out ice in summer. The model shows that if the summer albedo were reduced from the 0.64 used in the model to 0.54, the equilibrium thickness would fall to 1 m, and a further 0.1 reduction would cause the ice to melt completely. In practice, however, the artificial darkening of sea ice would probably not have such a drastic effect, as it would merely deepen the melt ponds, with much of the melt water refreezing again in autumn. Any effect big enough to cause basin-wide darkening of the ice, e.g. the fallout of material from an asteroid impact or a nuclear winter, would be so disastrous on a global scale that melting of Arctic sea ice would be one of the more trivial consequences.

A more obvious sensitivity is to air temperature T_a. The Maykut-Untersteiner model, and later heat balance models (Budyko, 1974; Parkinson and Kellogg, 1979), predict that summer air temperatures 4–5°C warmer than at present will result in an ice-free summer Arctic Ocean. Since such temperature rises are indeed predicted for the Arctic within the era of CO_2 doubling, i.e. the next 70 years (Cattle and Crossley, 1995), one might expect

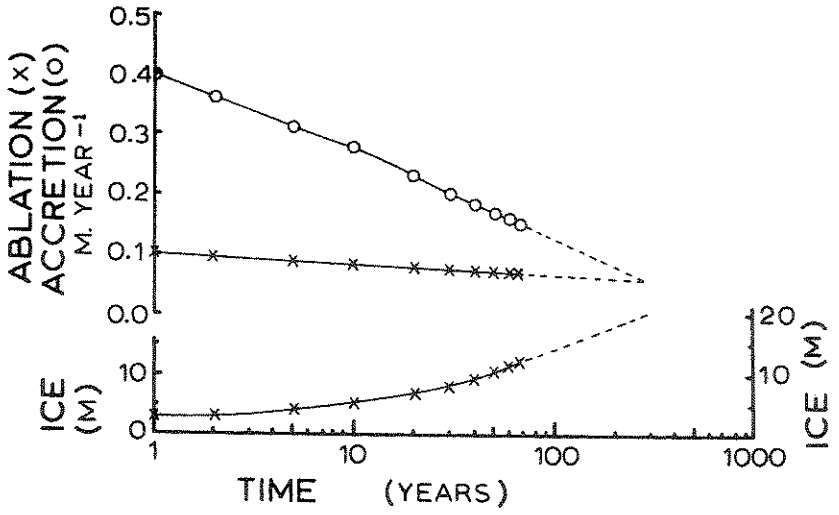

Figure 3.15. Ice thickness (m) and ablation and accretion rates (m yr^{-1}) achieved using Maykut-Untersteiner model with standard Arctic parameters except for an initial thickness of 3 m, an annual snowfall of 1 m, and no ocean heat flux. The extrapolated point at which ablation and accretion rates are equal gives the equilibrium thickness (after Walker and Wadhams, 1979).

that this will remove the ice from the Arctic. However, in reality a much more complex interaction will occur involving evaporation and the stability of the atmosphere over the ice; more complete coupled atmosphere-ocean models, such as that used in the general circulation model described by Cattle and Crossley (1995), predict an ice thickness loss of 1–1.5 m under this degree of warming.

Do special kinds of ice exist?

Given the sensitivity of ice thickness to ocean heat flux, snowfall and other factors, are there special circumstances anywhere in the world which allow ice to grow much thicker than expected? To simulate a coastal Arctic regime with a high local snowfall, Walker and Wadhams (1979) ran the Maykut-Untersteiner model with an oceanic heat flux set to zero and an annual snowfall increased to 1.0 m. The ice thickness (fig. 3.15) reached 12 m in 65 years. Extrapolation of the annual curves of ablation and accretion showed that an equilibrium thickness of 20 m would be eventually achieved after 200–300 years. Can we find ice of this kind?

There are a few isolated observations of thick undeformed floes in the Arctic Ocean. Cherepanov (1964) found that the 80 km^2 floe on which the Russian drifting station NP-6 had been established was 10–12 m thick, with a crystal structure which was typical of slow congelation growth. A 1 km floe of mean thickness 9.2 m, apparently undeformed, was observed by submarine sonar near the North Pole (Walker and Wadhams, 1979). A 10–12 m thick floe was observed by A R Milne (personal commun.) during an icebreaker

voyage west of Prince Patrick Island. However, on the whole, observations of thick floes are scarce in the drifting pack.

A clue to the possible origin of these thick floes came from observations in the Antarctic. During a winter experiment in 1986 aboard FS "Polarstern" a small number of floes of very high freeboard were observed in the pack (Wadhams *et al.*, 1987). Fig. 3.16 shows an example of such a floe. The origin of these floes was found to be bays along the edge of the nearby Fimbul Ice Shelf, from which icebergs had calved. The inlets "healed" themselves by growing multiyear fast ice. Protected from the drifting pack by the shelf edge geometry, the ice could keep growing from year to year with the special circumstances of high snowfall (mainly snow blown onto the ice surface by katabatic winds blowing over the ice shelf) and low oceanic heat flux (an outflow of very cold water from under the ice shelf). In this way the ice could reach 11 m or more, and the occasional small breakouts of ice from these fast ice regions produced the isolated thick floes seen in the drifting pack.

Could this account for very thick floes seen in the Arctic? There is indeed a type of very thick fast ice, first reported by Koch (1945) in north and northeast Greenland and given the Greenlandic Eskimo name **sikussak** ("fjord ice like ocean ice"). Koch reported three areas of sikussak in May 1938 in Peary Land (fig. 3.17), whereas in earlier years it had been more prevalent and had been responsible for holding calving icebergs in place against the edges of glaciers and preventing them from breaking out. In 1980 the author observed ice of sikussak type in the fast ice at the mouth of Danmarks and Independence Fjords in north Greenland (fig. 3.18, Wadhams, 1986). The ice had a highly developed surface drainage system, and a core drilled through 6.1 m of ice failed to reach bottom. A salinity record from the uppermost 4.6 m (fig. 3.19) shows evidence of many years of alternating growth and surface melt. In these fjords similar circumstances prevail as in the Antarctic ice shelf inlets: high snowfall (with high coastal mountains), low ocean heat flux (from the single-layer water structure in the fjord) and intensely cold air temperatures. Sikussak probably exists in other high Arctic coastal locations; for instance there have been observations of fast ice "plugs" of 10 m and 12 m in Nansen Sound and Sverdrup Channel in the Canadian high Arctic (Serson, 1972, 1974). The rare thick floes seen in the pack represent occasional break-outs from these source areas.

An intriguing possibility is that some ice that is conventionally viewed as shelf ice, i.e. ice of terrestrial origin, may really be very old fast sea ice, what may be termed super-sikussak. An Arctic example is the Ward Hunt Ice Shelf on the north of Ellesmere Island. Since the end of the Second World War this ice shelf has been progressively breaking up, giving rise to the famous **ice islands**, several km in diameter and 50 m or more thick, which have drifted in the Arctic Ocean and provided secure bases for research stations. The most famous of all was Fletcher's Ice Island T-3, which left the Beaufort Gyre in 1984 after 27 years and exited through Fram Strait, finally breaking up off SW Greenland. It is also possible that "islands" reported by early explorers north of Ellesmere Island, Peary's "Crocker Land" and Cook's "Bradley Land", were actually ice islands. Ward Hunt Ice Shelf is not actively fed by glaciers, unlike Antarctic ice shelves, and so is either a relic of the last glacial period or else, in whole or part, an accumulation of very thick, very slowly grown sea ice, with fabric properties resembling polycrystalline ice (including zero salinity) because of its very slow growth rate.

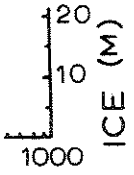

ıg Maykut-Untersteiner
ıl snowfall of 1 m, and
ıl gives the equilibrium

uch more complex
mosphere over the
ised in the general
ice thickness loss

l other factors, are
grow much thicker
l snowfall, Walker
eanic heat flux set
(fig. 3.15) reached
accretion showed
ter 200–300 years.

the Arctic Ocean.
lrifting station NP-
which was typical
rently undeformed,
Vadhams, 1979). A
ıring an icebreaker

(a)

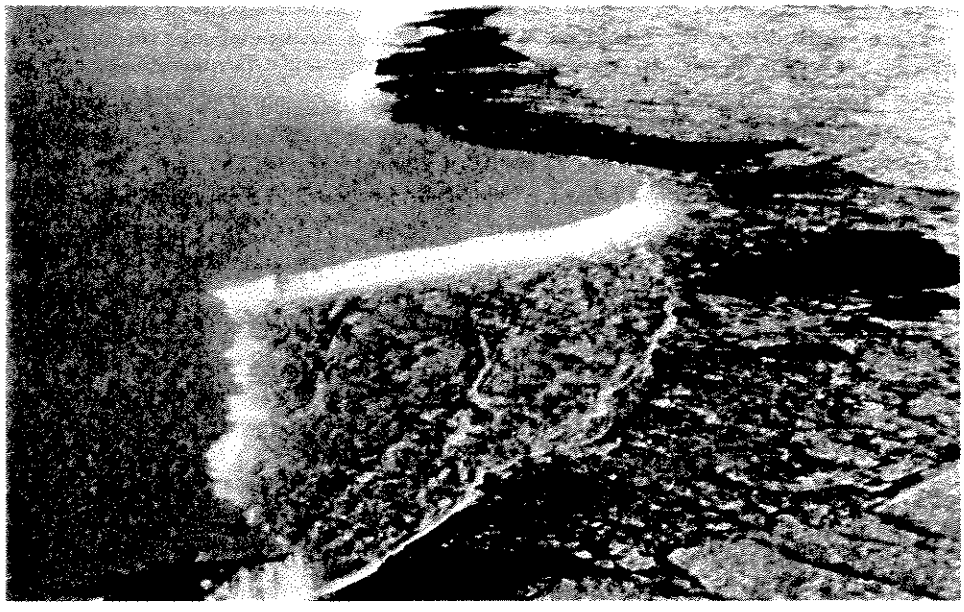

(b)

Figure 3.16. (a) Very thick floe observed embedded in first-year pack ice in eastern Weddell Sea during winter of 1986 (after Wadhams *et al.*, 1987). (b) A possible origin of these floes in thick fast ice formed within an embayment of the Fimbul Ice Shelf.

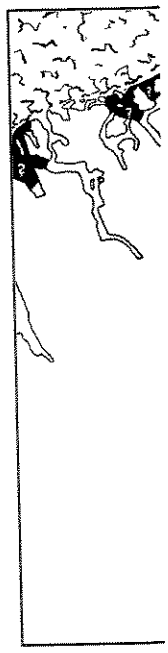

Figure 3.17. Map of sil

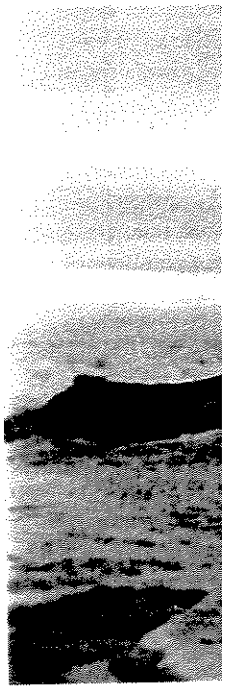

Figure 3.18. Ice of sik
1986).

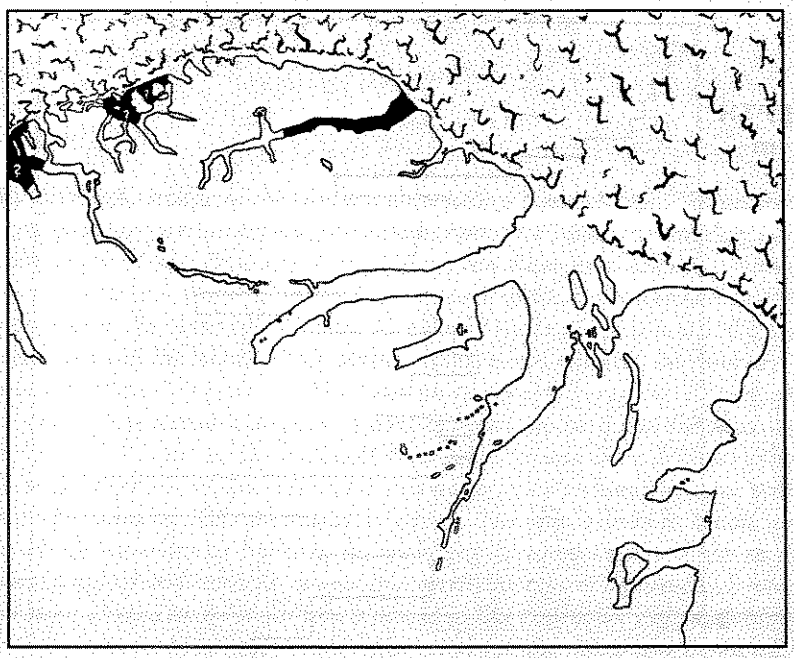

Figure 3.17. Map of sikussak occurrence in Peary Land, according to Koch (1945).

Figure 3.18. Ice of sikussak type observed by author in Independence Fjord, north Greenland (after Wadhams, 1986).

ll Sea during winter
e formed within an

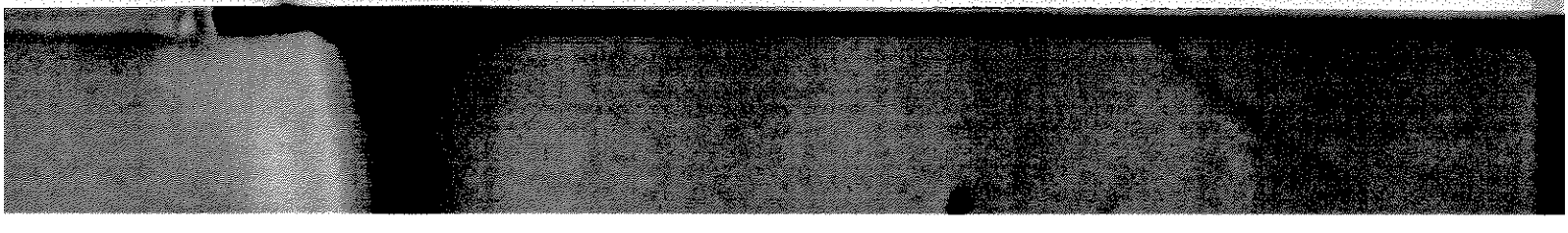

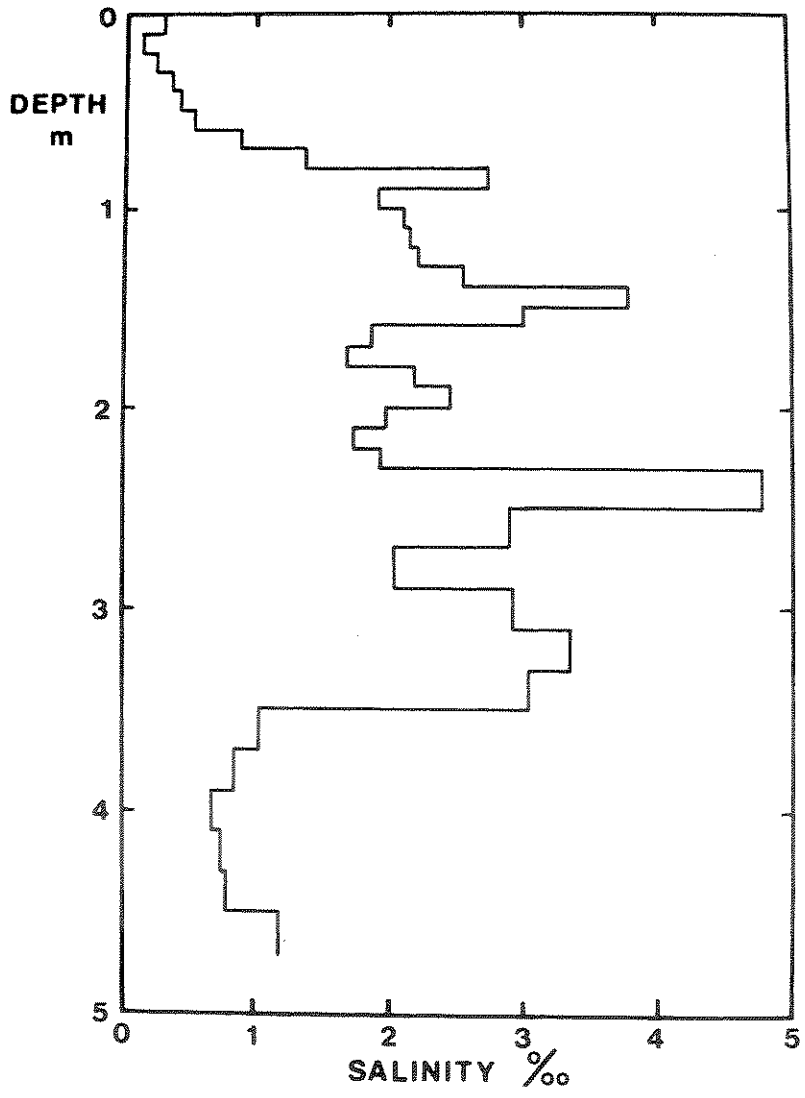

Figure 3.19. Salinity profile through part of core taken in sikussak, north Greenland (after Wadhams, 1986).

You are on the br
as she ploughs ec
coast towards Ai
A massive tabula
westward in the
detour around th
relieve the base?
the coast? The C
are excited. You
There are over 1(
accurate reading
for all her attem
She is trapped ar
has been ground
held together by
even this powerf
over the ship. Yo
decks are placea
would crash ont
much more slow
the coast. Everyc
and sunk. But yc
Closer it comes,
ship width. Ther
pressure is reliev
ice collapses bac
for Atka Bay.

At the end of chap
cover is affected by t
covering the sea surfa
coastal polynyas are e
go on to consider the
sea ice. Together with
the construction of ice
of thickness of an ice
Circulation Models (
behaviour of the globa
changes in which sea